

Synthesis, Spectroscopy, Nonlinear Optics, and Theoretical Investigations of Thienylethynyl Octopoles with a Tunable Core

María Moreno Oliva,^[a] Juan Casado,^{*,[a]} Juan T. López Navarrete,^{*,[a]}
Gunther Hennrich,^{*,[b]} Stijn van Cleuvenbergen,^[c] Inge Asselberghs,^[c] Koen Clays,^[c]
M. Carmen Ruiz Delgado,^[d] Jean-Luc Brédas,^[d] J. Sérgio Seixas de Melo,^[e] and
Luisa De Cola^[f]

Abstract: We have synthesized three new molecules that have three thienylethynyl arms substituting a central benzene core and different electron donor/acceptor groups in the three remaining phenyl positions. The absorption, fluorescence, phosphorescence, and transient triplet–triplet spectra are analyzed in the light of the electronic structure of the ground and excited states obtained from quantum-chemical calculations. From the above, the relevant photophysical data (including quantum

yields, lifetimes, and rate constants) could be derived. It was found that the major deactivation pathway is internal conversion, which competes with the fluorescence and intersystem crossing processes. For the three investigated compounds, we provide convincing the-

Keywords: density functional calculations • donor–acceptor systems • nonlinear optics • phosphorescence • sulfur heterocycles

oretical support corroborating these findings and further conclusions based on the theoretical information obtained. These molecules are one of the very few cases in which the depolarization ratios, obtained from the NLO optical measurements, clearly reflect the octopolar configuration. Molecular hyperpolarizabilities have been measured and display a typical dependence on the donor–acceptor substitution pattern.

Introduction

The synthesis of extended π -conjugated systems has been the key to providing organic materials with electro-optical properties needed for particular applications.^[1] Over the past few years, numerous synthetic routes have been investigated to optimize the molecular hyperpolarizabilities in octopolar molecules for nonlinear optical (NLO) response^[2] and, more recently, two-photon absorption (TPA) properties.^[3] Many of these organic systems present C_3 -symmetric architectures in which a central core is trigonally substituted with conjugated branches in between donor–acceptor groups and conjugative interactions with the center have been established. These types of dyes are also examples of molecules with π -electron delocalization extending in two dimensions (2D), which were recently successfully exploited as semiconductor elements in organic field-effect transistors and in light-emitting diodes.^[4] It is clear that the design of these molecules, or improved derivatives, must be founded on comprehensive knowledge of their electronic characteristics, in particular, their ground- and excited-state properties. For instance, it has been shown that donor–acceptor

[a] M. M. Oliva, Dr. J. Casado, Prof. J. T. López Navarrete
Department of Physical Chemistry, University of Málaga
Campus de Teatinos s/n, Málaga 29071 (Spain)
E-mail: casado@uma.es

[b] Dr. G. Hennrich
Departamento de Química Orgánica
Universidad Autónoma de Madrid
Cantoblanco, Madrid 28049 (Spain)
E-mail: teodomiro@uma.es

[c] Dr. S. van Cleuvenbergen, Dr. I. Asselberghs, Dr. K. Clays
Department of Chemistry, Katholieke Universiteit Leuven
Celestijnenlaan 200D and F, B-3001 Leuven (Belgium)

[d] Dr. M. C. Ruiz Delgado, Prof. J.-L. Brédas
School of Chemistry and Biochemistry and Center for Organic Photonics and Electronics, Georgia Institute of Technology
Atlanta, Georgia 30332-0400 (USA).

[e] Prof. J. S. Seixas de Melo
Department of Chemistry
University of Coimbra, 3004-535 Coimbra (Portugal)

[f] Prof. L. De Cola
Physikalisches Institut, Westfälische Wilhelms-Universität Münster
Mendelstrasse 7, 48149 Münster (Germany)

Supporting information for this article is available on the WWW under <http://dx.doi.org/10.1002/chem.200900702>.

strength, conjugation length, geometry, and nature of the relevant low-lying electronic states significantly influence the octopolar properties.^[2,5]

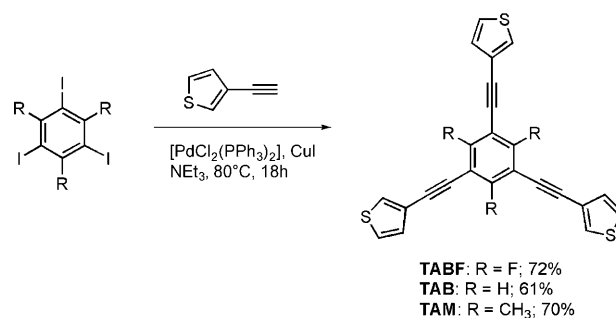
In the context of second-order nonlinear optics, one of the main arguments advanced in favor of such 2D octopolar molecules is the absence of a permanent dipole moment, in contrast to conventional linear systems that tend to self-assemble in an antiparallel manner.^[2] However, reaching non-centrosymmetric superstructures remains a crucial prerequisite that is not trivial to achieve.^[6] Recent accomplishments in the preparation of second-order NLO devices from crystalline^[7] and liquid-crystalline materials^[8] based on octopolar molecules have justified the expectations put into this kind of chromophores as active building units in electro-optical bulk materials.^[9]

In our quest to understand the structure–property relationships in these molecules, we combined a common benzene core trigonally substituted in the 1, 3, and 5 positions with terminal thienyl groups connected through an acetylene spacer. This spacer is recurrent because it offers efficient electronic communication within the molecular scaffold while minimizing the detrimental steric congestion at the same time.^[10] The central benzene core is substituted in its 2, 4, and 6 positions with methyl (donor) groups or fluorine (acceptor) atoms.

In continuation of our recent interest in C_3 octopoles,^[5] we report here on the photophysical properties of these thiophene-based systems. Special emphasis has been placed on characterizing the features of the main low-lying excited states intervening in the properties of interest. This work explores the absorption, steady-state and time-resolved emission (fluorescence and phosphorescence), and transient triplet–triplet absorption to account for the energies of the lowest-lying excited states together with the main excitation and relaxation routes in photoluminescence. Furthermore, we make use of vibrational Raman spectroscopy to scan the molecular structure of the electronic ground state. An additional section is devoted to the second-order nonlinear optical (NLO) response, as measured by hyper-Rayleigh scattering.^[11] The whole experimental study is guided by a theoretical analysis combining a variety of computational approaches, including Density Functional Theory and correlated Hartree–Fock-based methods. In the overall discussion, we put strong emphasis on the role of the excited electronic states of these conjugated octopolar molecules. Owing to the importance of these states for a variety of applications in organic electronic, this paper provides a perspective focused on the analysis of their features. The establishment of structure–property relationships is strongly pursued. To the best of our knowledge, there are few studies^[5] that utilize such a variety of spectroscopic tools, combined with theoretical predictions, all directed to elucidating the excited-state molecular properties.

Experimental and theoretical details

Materials and synthesis: The target compounds were obtained in good yields by three-fold Sonogashira coupling of the 1,3,5-triiodobenzene derivatives with 3-ethynylthiophene (Scheme 1).^[12]



Scheme 1. Synthesis of **TEB**, **TEM**, and **TEBF**.

General procedure for the synthesis of TEBF, TEB, and TEM: The respective 1,3,5-triiodobenzene (1.0 mmol) was stirred with [PdCl₂(PPh₃)₂]/CuI (0.15 mmol) in degassed diisopropylamine (10 mL) under argon at RT for 30 min before 3-ethynylthiophene (4.0 mmol) was added. After heating the mixture at 70 °C for 18 h, the solvent was evaporated, water (30 mL) added, and the mixture extracted with EtOAc (3 × 15 mL). The combined organic layers were dried over MgSO₄. The solvent was evaporated to leave the crude solid product, which was purified by recrystallization from the solvents specified below.

1,3,5-Tris(thienylethynyl)benzene (TEB): Recrystallization from toluene gave pure **TEB** as off-white crystals in 61% yield. $R_f = 0.57$ (20:1 hexanes/EtOAc); m.p. 196 °C; ¹H NMR (CDCl₃): $\delta = 7.60$ (s, 3H), 7.55 (m, 3H), 7.33–7.19 ppm (m, 6H); ¹³C NMR: $\delta = 133.7, 129.8, 129.1, 125.5, 124.0, 121.8, 87.3, 85.6$ ppm; (EI⁺-HRMS): m/z : calcd for C₂₄H₁₂S₃: 396.0101; found: 396.0103.

1,3,5-Tris(thienylethynyl)mesitylene (TEM): Recrystallization from toluene/EtOH (5:1) gave pure **TEM** as colorless crystals in 70% yield. $R_f = 0.52$ (20:1 hexanes/EtOAc); m.p. 216 °C; ¹H NMR (CDCl₃): $\delta = 7.55$ –7.53 (m, 3H), 7.35–7.31 (m, 3H), 7.24–7.21 (m, 3H), 2.71 ppm (s, 9H); ¹³C NMR: $\delta = 141.8, 129.7, 128.2, 125.4, 122.5, 121.2, 92.3, 86.3, 20.3$ ppm; (EI⁺-HRMS): m/z : calcd for C₂₇H₁₈S₃: 438.0571; found: 438.0553.

1,3,5-Tris(thienylethynyl)-2,4,6-trifluorobenzene (TEBF): Recrystallization from CH₃CN gave pure **TEBF** as pale purple crystals in 72% yield. $R_f = 0.52$ (20:1 hexanes/EtOAc); m.p. 194–196 °C; ¹H NMR (CDCl₃): $\delta = 7.56$ –7.55 (m, 3H), 7.27–7.24 (m, 3H), 7.18–7.15 ppm; ¹³C NMR: $\delta = 161.8$ (d), 131.2, 130.1, 129.7, 125.6, 120.8, 95.0, 73.5 ppm; (EI⁺-HRMS): m/z : calcd for C₂₄H₉F₃S₃: 449.9819; found: 449.9818.

Spectroscopic measurements: Absorption and fluorescence spectra were recorded on Shimadzu UV-2100 and Horiba–Jobin–Ivon SPEX Fluorog 3-22 spectrometers, respectively. The fluorescence spectra were corrected for the wavelength response of the system. The fluorescence quantum yields were measured using bithiophene ($\Phi_F = 0.014$ in methylcyclohexane)^[13] as the standard. Fluorescence decays were measured using a home-built TCSPC apparatus described elsewhere^[14] and were analyzed using the modulating functions method of Striker.^[15] The experimental setup used to obtain triplet spectra and triplet yields has been described elsewhere.^[14,16] First-order kinetics were observed in all cases for the decay of the lowest triplet state, and the lifetime values were in the μ s range. When determining the triplet yields, special care was taken to have optically matched dilute solutions (abs ≈ 0.2 in a 10 mm square cell) and low laser energy (≤ 2 mJ) to avoid multiphoton and T–T annihilation effects. The triplet molar absorption coefficients were obtained by the singlet-depletion and energy-transfer methods. Details of the experimental procedures and data analysis used can be found in Refs. [14,16]. Room-temperature singlet-oxygen phosphorescence was detected at

1270 nm with the equipment and procedures reported elsewhere.^[14,16] The singlet-oxygen quantum yields were obtained from these signals. Thin films were obtained with a Desk-Top Precision Spin Coating System, Model P6700 Series from Speedline Technologies with procedures reported elsewhere.^[14,16] The fluorescence emission spectra of the thin films were obtained with a Horiba-Jobin-Yvon integrating sphere. The solid-state photoluminescence quantum yields in thin films were obtained as previously described.^[14,16]

FT-Raman spectra (1064 nm) were measured using an FT-Raman accessory kit (FRA/106-S) and a Bruker Equinox 55 FT-IR interferometer. A continuous-wave Nd-YAG laser working at 1064 nm was employed for excitation. A germanium detector operating at liquid nitrogen temperature was used. Raman scattering radiation was collected in a back-scattering configuration with a standard spectral resolutions of 4 and 1 cm⁻¹; 1000–3000 scans were averaged for each spectrum. A variable-temperature cell Specac P/N 2100, with interchangeable pairs of quartz windows, was used to record the FT-Raman spectra at different temperatures.

Quantum-chemical calculations: Depending on the specific spectroscopic property addressed, a variety of theoretical methodologies have been used. Density functional theory is very well suited for the study of π -conjugated molecules, in which electron correlation plays a significant role.^[17] DFT has been used for the ground-state properties (i.e., optimized geometries, vibrational spectra, etc.), and its time-dependent extension TD-DFT has been used to estimate the vertical and adiabatic excited-state transitions (i.e., energies and oscillator strengths).^[18] DFT also provides reliable geometry optimizations of the lowest triplet state (i.e., T₁), whereas TD-DFT can be used to address vertical transitions within the triplet manifold. In order to evaluate the optimized geometries of higher-lying excited states, we have relied on the restricted configuration interaction with singles approach (CIS) within the Hartree-Fock (HF) approximation (RCIS/HF) in which the single determinant RHF wavefunction is used as the reference determinant in a CIS calculation of excited states.^[19]

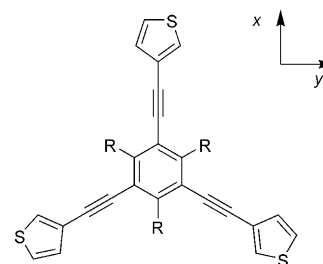
Most of the computations were performed with the Gaussian03 package.^[20] The DFT calculations were based on Becke's three-parameter gradient-corrected exchange functional combined with the Lee-Yang-Parr correlation functional (B3LYP).^[21] The 6-31G** basis set was used in all DFT and HF calculations.^[22] The T₁ state was optimized at the DFT level with the corresponding unrestricted methodology (i.e., UB3LYP/6-31G**). The molecular geometries of the ground state (excited states) were optimized assuming C_{3h} (C₃) symmetry. In the TD-DFT calculations, at least the ten lowest-energy vertical electronic excited states were evaluated. TD-DFT calculations were performed with the same functional (B3LYP) and basis set (6-31G**). Using the ground-state optimized geometries, the harmonic vibrational frequencies and Raman intensities were calculated analytically at the DFT/B3LYP/6-31G** level.

Nonlinear optics calculations: Based on DFT/B3LYP/6-31G** ground-state optimized geometries, the second-order polarizabilities (β) were evaluated with the semiempirical Intermediate Neglect of Differential Overlap (INDO) Hamiltonian.^[23] The spectroscopic parameterization, along with the Mataga-Nishimoto^[24] electron-repulsion potential, was used, as implemented in the ZINDO code.^[25] For sum-over-states (SOS) hyperpolarizabilities (see, e.g., Ref. [26] for the standard expressions), the electronic properties of the ground and electronically excited states (transition energies, state and transition dipole moments) were evaluated using two configuration interaction schemes. The first considered singly excited configurations (SCI) with an active space that included all occupied and unoccupied π -molecular orbitals (MO's). We note that INDO calculations coupled to a SCI Scheme have been shown to provide reliable descriptions of the second-order polarizabilities.^[26] The second was based on a SDCI (single and double configuration interaction) approach that included single excitations between all occupied and unoccupied π -MO's as well as double excitations among the five highest occupied π -MO's and five lowest unoccupied π^* -MO's.

The components of the static β tensor along the x axis (β_{xxx}) were also calculated using the Finite Field (FF) approach, in its local contribution version,^[27] as proposed by Chopra et al.^[28] and developed by Nakano et al.^[29] Geskin and co-workers have successfully applied this method to

conjugated organic systems in conjunction with the INDO Hamiltonian.^[30] The FF approach relies on the fact that, by definition, β_{xxx} is the second derivative of the x component of the dipole moment μ_x with respect to the x components of the applied electric fields (F) at zero field. The electronic part of β can be cast rigorously as the integral over the moments of the second derivative of the charge density ρ . In an approximate way, that integral can be partitioned into a sum over derivatives of point charges q_i concentrated on the individual atoms i

$$\beta_{xxx} = \left. \frac{\partial^2 \mu_x}{\partial F_x^2} \right|_{F_x=0} = \int x \left. \frac{\partial^2 \rho(r)}{\partial F_x^2} \right|_{F_x=0} d^3 r = \sum_i x_i \left. \frac{\partial^2 q_i^2}{\partial F_x^2} \right|_{F_x=0} = \sum_i x_i q_i^{(2)} \quad (1)$$



Here, β_{xxx} is partitioned into local (atomic) contributions or so-called β moments $x_i q_i^{(2)}$ derived from the β charges $q_i^{(2)}$. Note that the superscript (2) represents the second derivative with respect to the applied electric field in the x direction (with the x subscript dropped to simplify the notation). In this work, the charge derivatives were approximated by finite differences obtained from INDO Mulliken charges, with fields of zero and $\pm 5.14 \times 10^{11}$ V m⁻¹ (10^{-3} atomic units) applied to the octopolar molecules.

Results and Discussion

Absorption spectra: Figure 1 displays the absorption and emission spectra of the investigated compounds. TD-DFT excited-state calculations helped us assign the experimental bands (Figure 2a).

Figure 1 and 2 and Table 1 show that, for example for **TEBF**, the lowest energy, and strongest, band at 302 nm, corresponds to the degenerate theoretical S₀→S₂ and S₀→S₃ transitions predicted at $\lambda = 315$ nm. This band is followed at higher energies by a medium intensity band at $\lambda = 291$ nm due to the degenerate S₀→S₅/S₀→S₆ transitions calculated at $\lambda = 295$ nm and by the strong band measured at $\lambda = 287$ nm arising from the S₀→S₇+S₀→S₈ excitations estimated theoretically at $\lambda = 281$ nm.

In Figure 2a, a comparison of the experimental and theoretical spectra highlights the relative experimental intensity and oscillator strength of the three relevant bands for **TEBF**. Even though these electronic excitations are best described by multi-electron promotions involving their frontier orbitals, some parallel tendencies can be extracted: i) The theoretical HOMO-LUMO energy gaps in Figure 3 and the experimental optical ones evolve similarly: the former as 4.21 eV in **TEBF**, 4.26 eV in **TEB**, and 4.17 eV in **TEM**; the second as 4.09 eV in **TEBF** (i.e., 303 nm)→4.08 eV in **TEB** (i.e., $\lambda = 304$ nm)→4.03 eV in **TEM** (i.e., $\lambda = 308$ nm). Hence, theory predicts the narrowest gap for **TEM** to coincide with

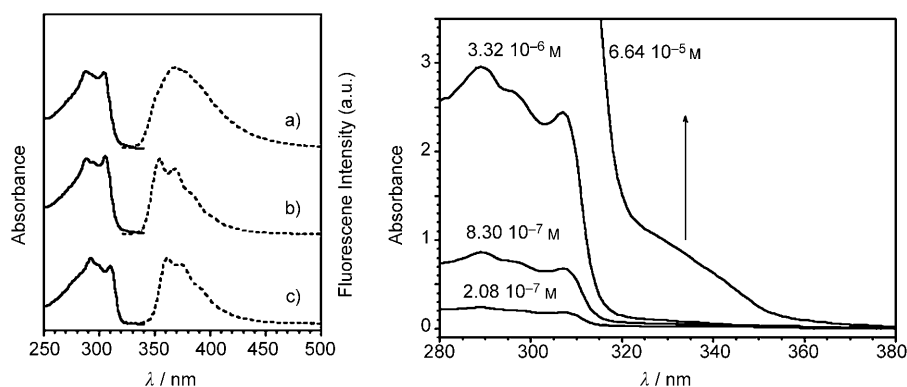


Figure 1. Left: absorption and emission spectra in CH_2Cl_2 for $\approx 10^{-4}\text{ M}$ solutions of a) **TEM**, b) **TEB**, and c) **TEBF**. Right: absorption spectrum of **TEM** at different concentrations in cyclohexane obtained with cuvettes with a pathlength of 100 mm.

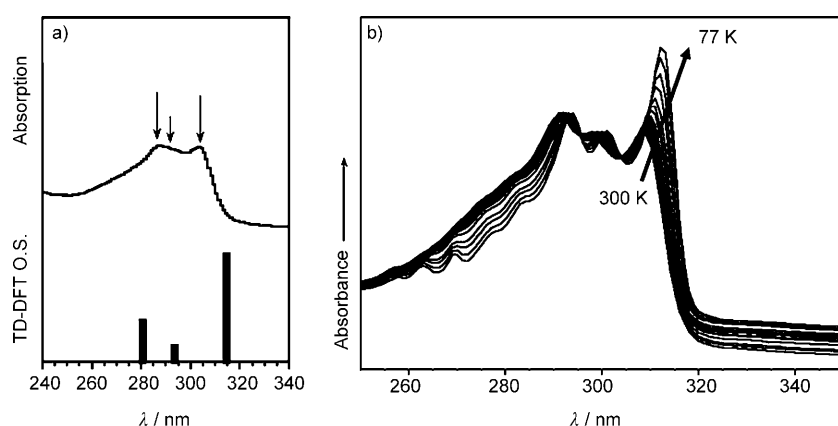


Figure 2. a) TD-DFT//B3LYP/6-31G** theoretical (bars) and experimental spectra of **TEBF** (in CH_2Cl_2). b) Spectrum of **TEM** on cooling from room temperature to 77 K (in butyronitrile).

Table 1. Photophysical data in methylcyclohexane and nonlinear optical data in CH_2Cl_2 at 300 K.^[a]

	$\lambda_{\text{max}}(\text{abs})$ [nm]	$\log(\epsilon)$	$\lambda_{\text{max}}(\text{em})$ [nm]	Φ_{fl}	τ_{fl} [ns]	$\beta_{\text{xxx},800}^{\text{[a]}}$ [10^{-30} esu]	$\beta_{\text{xxx},0}^{\text{[b]}}$ [10^{-30} esu]	$\rho^{\text{[c]}}$
TEB	290 (313)	4.813	358	0.15	8.0 ± 0.1	16 ± 1	7 ± 1	1.14 ± 0.03
TEM	294 (317)	4.822	366	0.10	9.2 ± 0.1	26 ± 3	11 ± 1	1.17 ± 0.05
TEBF	290 (315)	4.785	372	0.07	2.2 ± 0.1	59 ± 3	21 ± 1	1.55 ± 0.03

[a] $\beta_{\text{xxx},800}$ are the dynamic hyperpolarizability values at 800 nm. [b] $\beta_{\text{xxx},0}$ are the static hyperpolarizability values. [c] ρ denotes the depolarization ratio in the NLO measurements. See the NLO section for additional details.

the most red-shifted bands, experimentally measured at $\lambda = 308$ nm (i.e., 4.03 eV) in **TEM** as well. ii) Also seen in Figure 3, the HOMO and HOMO-1 levels are particularly destabilized in **TEM** by 0.22 and 0.28 eV, respectively, relative to those in **TEB** and **TEBF**, thus providing information on the positive inductive effect (i.e., +I) of the methyl groups and on the negative or electron-withdrawing effect of the three central fluorine atoms. iii) The same effects produce a stabilization/destabilization of the LUMO (and LUMO+1) orbitals in **TEBF/TEM** relative to **TEB**. iv) A distinctive feature of the wavefunctions of the frontier orbi-

tals (HOMO-1, HOMO, LUMO and LUMO+1) of **TEBF** relative to its counterparts is the larger participation of the fluorine atoms, seemingly consisting of a reorganization of the charge in these atoms along with the excitation (i.e., HOMO \rightarrow LUMO+1 or HOMO-1 \rightarrow LUMO promotions) that can be related to a certain charge-transfer property in **TEBF**. This argument will be invoked in the NLO section as well as in the Raman characterization.

Theory predicts the first excited state to appear at $\lambda \approx 330$ nm and to be radiatively decoupled from the ground electronic state. The $S_0 \rightarrow S_1$ transition is forbidden by the dipole-dipole optical selection rules for the C_{3h} geometry. In order to experimentally observe this forbidden transition, spectra were recorded in solution for different **TEM** concentrations (in cuvettes with a 100 mm path length), see Figure 1b, and a reproducible band at $\lambda = 332$ nm was obtained with an extinction coefficient of $1560\text{ M}^{-1}\text{ cm}^{-1}$. Distortion from the C_{3h} planar geometry in solution can be expected to contribute to the activation of this band.

Inspection of the evolution of the absorption spectra as a function of temperature for **TEM** reveals an enhancement of the $\lambda = 308$ nm band relative to the other two (Figure 2b). The lowest temperature spectrum is more similar to the theoretical one in terms of relative intensities (Figure 2a).

The FT-Raman spectra of these samples in the solid state at low temperatures display a continuous blue shift of the whole spectrum on cooling to -170°C . This is interpreted as an intermolecular effect and rules out a possible intramolecular structural or ground electronic state effect (see the section on vibration Raman spectra below). In the next discussion, we will see that the S_2/S_3 excited states feature electron delocalization along the acetylene bridge and subsequent rigidification (cumulenic character). This is favored by intermolecular solute-solvent interactions at low temperature that

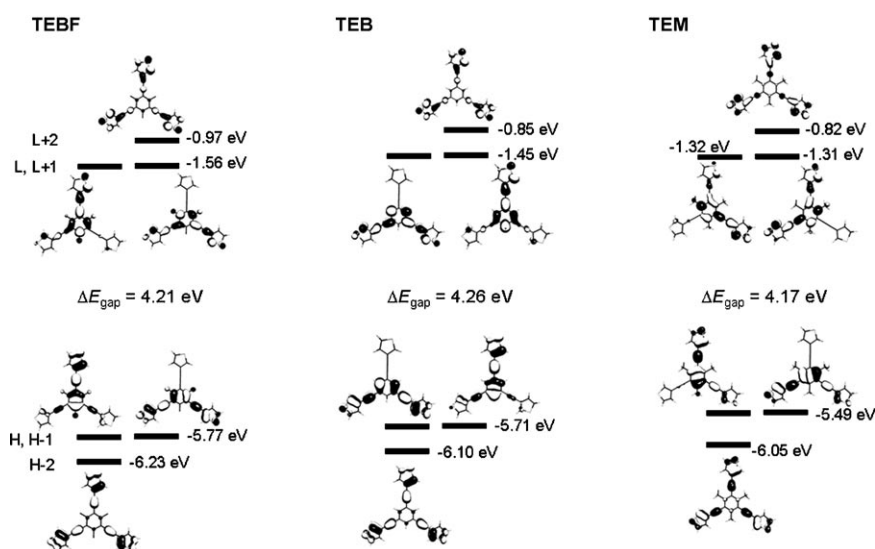


Figure 3. DFT/B3LYP/6-31G** wavefunction topologies of the orbitals around the gap.

probably improve the vertical alignment of the ground and excited states, thus intensifying the $S_0 \rightarrow S_2/S_3$ transition.

Fluorescence spectra—the singlet states: Figure 1a shows the absorption and fluorescence spectra of the three octopoles, and Table 1 summarizes the relevant spectral and photophysical data. Table 2 presents the spectral characteristics in the nonpolar solvent methylcyclohexane, including singlet and triplet extinction coefficients, and Table 3 gives the remaining photophysical parameters and rate constants, including singlet-oxygen sensitization yields.

The bathochromic displacement $\lambda = 358 \rightarrow 366 \rightarrow 372$ nm observed for the sequence **TEB** \rightarrow **TEM** \rightarrow **TEBF** together with the gradual loss of vibrational structure of the emission bands follows the expected trend in terms of enhanced charge-transfer character (**TEBF** $>$ **TEM** $>$ **TEB**). From the absorption and fluorescence spectra of **TEM**, **TEB**, and **TEBF**, a significant displacement of the absorption relative to the emission maxima [Stokes shift (SS)], can be observed.

Table 2. Spectral characteristics in methylcyclohexane at 293 K and 77 K.

	$\lambda_{\max}(\text{abs})^{293\text{K}}$ [nm]	$\lambda_{\max}(\text{exc})^{77\text{K}}$ [nm]	$\lambda_{\max}(\text{em})^{293\text{K}}$ [nm]	$\lambda_{\max}(\text{em})^{77\text{K}}$ [nm]	ϵ_S [$\text{M}^{-1}\text{cm}^{-1}$]	ϵ_T [$\text{M}^{-1}\text{cm}^{-1}$]
TEB	290	290	358	354	65 900	47 009
TEM	294	291	366	357	63 160	44 482
TEBF	290	290	372	365	65 080	50 435

Table 3. Photophysical parameters and rate constants in methylcyclohexane.

	$\Phi_f^{77\text{K}}$	Φ_Δ	Φ_T	$\Phi_{\text{IC}}^{[a]}$	k_T [s^{-1}]	τ_T [s]	$k_F^{[b]}$ [ns^{-1}]	$k_{\text{NR}}^{[c]}$ [ns^{-1}]	$k_{\text{ISC}}^{[d]}$ [ns^{-1}]	$k_{\text{IC}}^{[e]}$ [ns^{-1}]
TEB	0.17	0.30	0.28	0.57	4.05×10^4	2.47×10^{-5}	0.012	0.11	0.04	0.08
TEM	0.15	0.31	0.30	0.60	3.20×10^5	3.13×10^{-6}	0.013	0.10	0.03	0.06
TEBF	0.20	0.29	0.27	0.66	4.37×10^4	2.29×10^{-5}	0.06	0.40	0.13	0.27

[a] $\Phi_{\text{IC}} = 1 - \Phi_F - \Phi_T$. [b] $k_F = \frac{\Phi_F}{\tau_F}$. [c] $k_{\text{NR}} = \frac{1 - \Phi_F}{\tau_F}$. [d] $k_{\text{ISC}} = \frac{\Phi_T}{\tau_F}$. [e] $k_{\text{IC}} = \frac{\Phi_{\text{IC}}}{\tau_F}$.

This suggests that the geometries of the S_0 and S_1 states are either significantly different or that the absorbing and emitting states are not the same. We note that upon cooling to 77 K, the maxima and shape of the emission spectra do not change significantly (see Figure S1), thus indicating that the emitting states are the same (identical potential energy curves) at 293 K and 77 K. Because the weak dipole-dipole forbidden $S_0 \rightarrow S_1$ transition of **TEM** is located at $\lambda = 332$ nm and the $S_1 \rightarrow S_0$ emission is found at 366 nm, the SS is much smaller and confirms the different nature of the main transitions in absorption ($S_0 \rightarrow S_2$) and

emission ($S_1 \rightarrow S_0$; Figure 1b).

The vibrational structure of the emission spectra remains practically unchanged from 293 K to 77 K, which is compatible with a planar quinoidal-like structure for the active excited state.^[27] The following arguments are also in accordance with the discussion above: i) For **TEB**, the $S_1 \rightarrow S_0$ theoretical energy is calculated at 347 nm close to the experimental value at 358 nm in CH_2Cl_2 . ii) Fluorescent quantum yields are rather small and are therefore also in agreement with the small electronic coupling between the S_0 and S_1 electronic states. iii) The evolution of the fluorescence quantum yields in the three octopoles can be accounted for by a competition between internal conversion and the intersystem (ISC) crossing between S_1 and the closest triplet state. In fact, ISC to the triplet manifold is one of the main routes proposed to quench the fluorescence in thiophene derivatives, thus we have calculated the vertical and adiabatic energy positions of the first triplet and singlet excited states by TD-DFT (Figure 4). ISC is likely to take place between

S_1 and the closest triplet state of lower energy; in this context, the $S_1 \rightarrow T_7$ ISC process is calculated to be the most probable. When measuring the quantum yield Φ_T for the ISC process, the values are found to be rather similar for all three molecules (Table 3). These results are well supported by the similar exchange energy, or $\Delta(S_1 - T_7)$, predicted theoretically by TD-DFT to be 0.07, 0.07/0.06 eV in **TEB**, **TEM/TEBF**. In this regard, internal conversion seems to control the fluorescence efficiency because in 1,2-

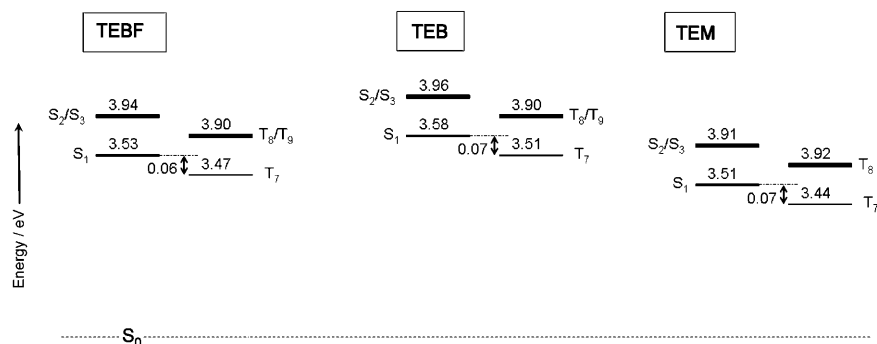


Figure 4. TD-DFT//B3LYP/6-31G** excited-states energies in the singlet and triplet excited-state manifolds.

dichloromethane and methylcyclohexane at room temperature the less fluorescent molecule, **TEBF**, displays the largest internal conversion quantum yield. At 77 K, however, **TEBF** turns out to have the greatest fluorescence quantum yield, indicating a more prominent blocking of the IC radiationless channel on cooling in the molecule with the largest fraction of it ($\Phi_{IC}=0.66$) at room temperature (Table 3).

The fluorescence decays obtained with nanosecond time resolution were found to be single exponential. Moreover, they remain mono-exponential on the ps timescale, indicating that no energy transfer or conformational relaxation processes occur on this timescale, which supports the “rigid” nature of the S_1 emitting state.

Phosphorescence spectra—the triplet state: As discussed above, the ISC process competes with fluorescence and internal conversion. This prompted us to explore the optical properties of the triplet manifold by measuring the phosphorescence spectra and performing flash photolysis in non-polar solvents (see below). The phosphorescence spectra at 77 K are shown in Figure 5, and Table 4 summarizes the corresponding data.

Figure 6 highlights the good correlation between the experimental and theoretical energies for the three relevant excited electronic states, which further supports the use of computational modeling in the following discussion. The greatest difference between the phosphorescence maxima is $7/0.04 \text{ nm eV}^{-1}$ [i.e., $475/2.61 \text{ nm eV}^{-1}$ in **TEBF**, $477/2.60 \text{ nm eV}^{-1}$ in **TEM**, and $482/2.57 \text{ nm eV}^{-1}$ in **TEB**] whereas for fluorescence the corresponding difference is 14 nm;

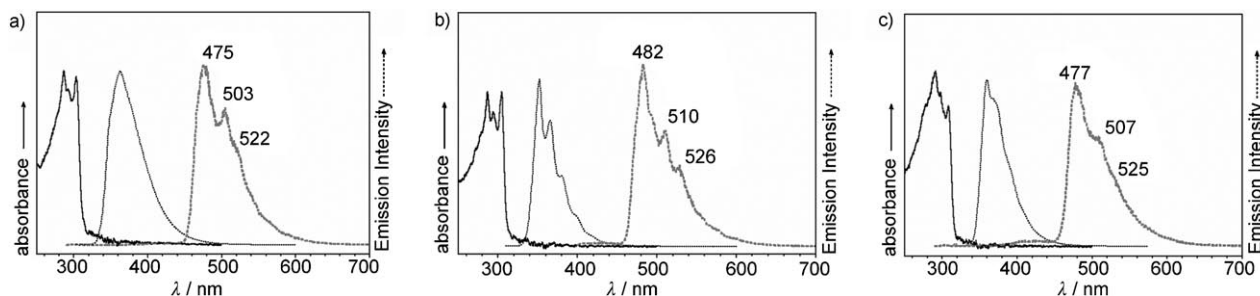


Figure 5. Absorption (293 K), fluorescence (293 K), and phosphorescence (77 K, grey) spectra in methylcyclohexane of a) **TEBF**, b) **TEB**, and c) **TEM**.

this indicates that in the T_1 state the electron delocalization is less pronounced or restricted to a smaller molecular domain compared to the S_1 state. This is illustrated in Figure 7, which shows the theoretical structures of these excited states, and is in accordance with previous data.^[31]

The electronic structure of the S_1 state displays symmetri-

Table 4. Phosphorescence data in methylcyclohexane at 77 K.

	$\lambda_{\text{max}}(\text{em})$ [nm]	Φ_{phos}	τ_{phos} [ms]
TEM	477, 507, 525	0.10	284
TEB	482, 510, 526	0.11	363
TEBF	475, 503, 522	0.15	387

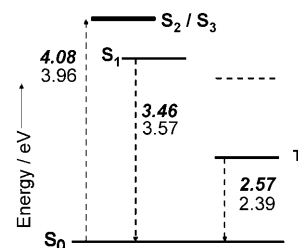


Figure 6. Energy diagram for the electronic singlet and triplet states of **TEB** comparing experimental (bold italics) and theoretical data.

cal distortion around the central benzene core and has an equal effect on the acetylene arms and more slightly on the peripheral thiophene rings; however, the T_1 state is far more similar to the S_2/S_3 states and is mainly located in one of the three arms. These states are characterized by a *cumulenic* character within the acetylene spacer and an asymmetrical quinoidization of the central benzene ring. As a significant difference between the T_1 and S_2/S_3 states, the former is centered on the acetylene spacer with a stronger *cumulenic* character. Hence the thiophene rings are less affected in T_1

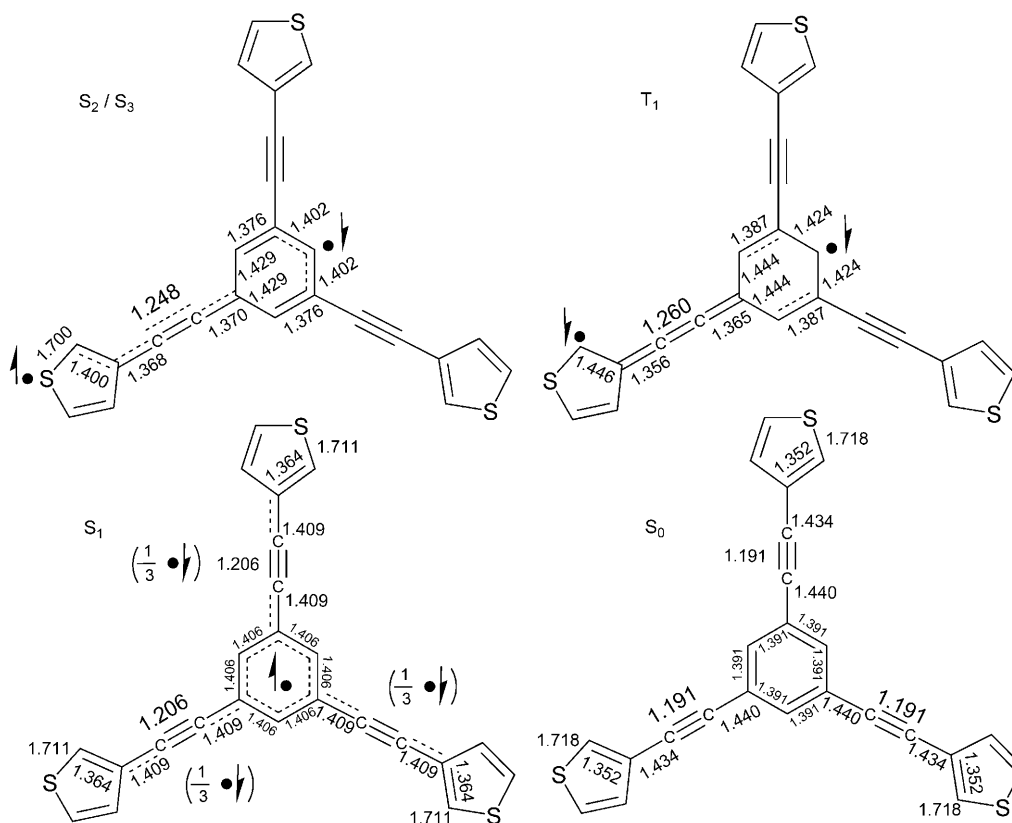


Figure 7. Representation of the geometric/chemical structures of the excited states of **TEB** as deduced from RCIS/6-31G** calculations. The optimized geometry of the ground state (S_0) was calculated with DFT//B3LYP/6-31G**. Bond lengths are given in Å.

than in S_2/S_3 with these high-energy singlets readily involving the sulfur atoms of the outermost thiophenes. This theoretical consideration is in very good agreement with the structural properties deduced from the above experimental optical features relative to the different shifts of the fluorescent/phosphorescent emissions in the three molecules. The participation of the sulfur atoms in the optically relevant frontier orbitals results in the heavy atom effect coming into play,^[32] which can lead to spin flipping in the ISC process. In any case, an additional mechanism for spin-orbit coupling will be discussed in the following paragraph.

The three compounds display high phosphorescence quantum yields. The case of **TEBF** is remarkable because the largest phosphorescence quantum yield (i.e., 0.15) is observed in the molecule where ISC is most favored. For acetylene derivatives, rapid intersystem crossing is expected because of the presence of two π -orbitals, π_1 and π_2 , that are perpendicular to each other; one conjugates strongly with the phenyl and thiophene rings, whereas the other is mainly localized on the acetylene bonds. Due to the π_1 - π_2 configuration, the excited state will contribute to enhancing the spin-orbit coupling responsible for intersystem crossing.^[32,33]

There is vibronic structure in the three phosphorescence spectra. The peak spacing in this vibrational structure is around 1100–1300 cm^{-1} , which corresponds to vibrations of the acetylene spacer, in particular, stretches of the single C–

C bonds, $\nu(\text{C-C})$. These bonds are especially affected on excitation at the origin of the vibronic activity.

TD-DFT calculations provide the theoretical energy for the $S_0 \rightarrow T_1$ transitions, which would relate with the phosphorescence wavelengths. For instance, in **TEB**, this transition is predicted at 518 nm, in agreement with the set of sub-peaks at 482/510/526 nm. This correlation provides further support for the assignment of the low-temperature emission to phosphorescence.

Transient triplet–triplet absorption spectra and yields: The transient triplet–triplet absorption spectra in Figure 8 display a depletion at ≈ 300 nm followed by a maximum at ≈ 500 nm.

In order to assess the transient spectra in terms of triplet–triplet transitions, we have calculated the TD-DFT//UB3LYP/6-31G** transitions starting from the DFT//UB3LYP/6-31G** T_1 geometry. These theoretical results are shown in Figure 9 for **TEB** compared with the corresponding flash-photolysis spectrum taken 0.39 μs after excitation.

In our experimental interval, the most active and optically relevant transitions are recorded for these samples. It must be pointed out that these bands involve relatively high energy excitations where, very usually, theoretical calculations such as TD-DFT fail in the estimation. Thus, while

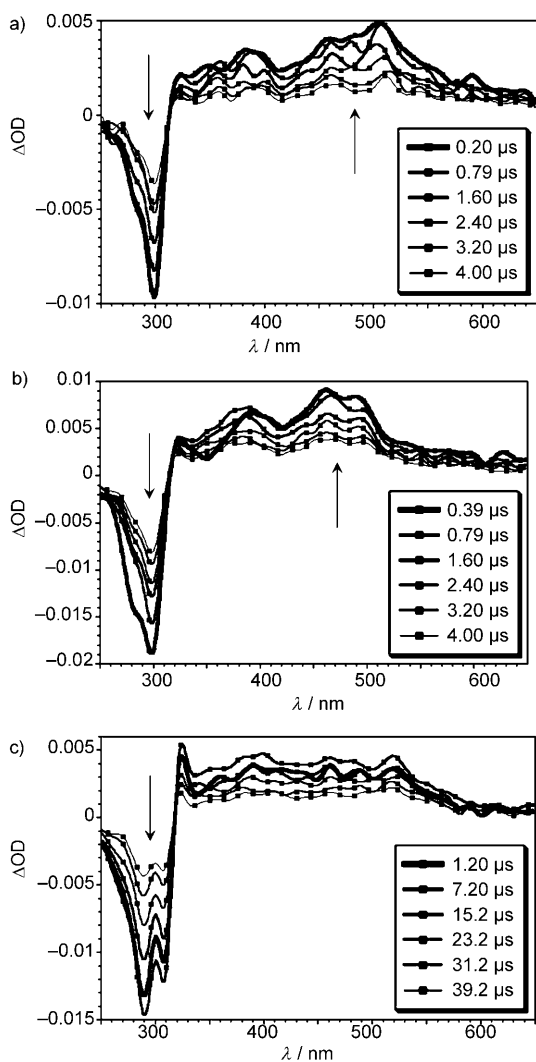


Figure 8. Transient triplet-triplet spectra of the investigated octopolar compounds in methycyclohexane at room temperature (293 K). a) **TEBF**, b) **TEB**, and c) **TEM**

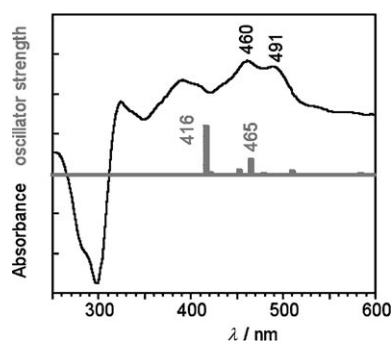


Figure 9. Transient triplet-triplet spectrum of **TEB** in methycyclohexane recorded 0.39 μs after excitation (black line) and its theoretical TD-DFT//UB3LYP/6-31G** triplet-triplet spectrum (grey).

considering this correlation with much caution, we suggest that the pair of bands at 460/491 nm could be related to those calculated at 416/465 nm, which correspond, respec-

tively, to $T_1 \rightarrow T_{19}$ and $T_1 \rightarrow T_{14}$ triplet-triplet transitions; in addition, these two bands are the strongest predicted transitions.

The ISC yield values indicate that ISC is an efficient decay channel for S_1 . The quantum yields for singlet-oxygen sensitization are practically identical to the ϕ_T values (Table 3), thus supporting these considerations and showing that the compounds efficiently sensitize molecular singlet oxygen. In addition, the nature of the T_1 state could be inferred from the phosphorescence lifetimes, whose values are indicative of allowed π, π^* triplet states.^[32-34] This is corroborated theoretically because the $S_0 \rightarrow T_1$ excitation corresponds to the HOMO \rightarrow LUMO dipole-forbidden transition with two orbitals of π -character, as discussed previously. The ϕ_{phos} values show that these compounds are moderately phosphorescent (10% of the deactivation), which is uncommon for thiophene compounds, although it has been observed for terthiophene derivatives using gated detection in combination with nanosecond excitation in frozen solutions at 80 K.^[31] The photophysical parameters in Table 3 show that the radiationless internal conversion dominates the deactivation of the S_1 state over the radiative and ISC processes because the sum $\Phi_F + \Phi_T$ only accounts for 0.3–0.4 (Table 3). However, from the rate constant values (k_F , k_{ISC} , k_{IC}), the three processes are kinetically competitive with values of the same order of magnitude (Table 3). From the molar extinction coefficients of the $S_0 \rightarrow S_1$ transitions and the k_F values it is clear that S_1 and S_2 are of π, π^* origin, although in the first case $S_0 \rightarrow S_1$ is symmetry forbidden (Tables 2 and 3).

Solid-state electronic spectra: Studies carried out in dilute solution essentially probe intramolecular excitations. However, it has become evident that the optical properties of conjugated molecules are greatly affected by intermolecular interactions that are predominant in the solid state.^[35] Consequently, optical data from solid thin films are more likely to reflect the excitation dynamics present in electroluminescent devices. Figure 10 displays the absorption and emission spectra (fluorescence and phosphorescence) of **TEM** in the

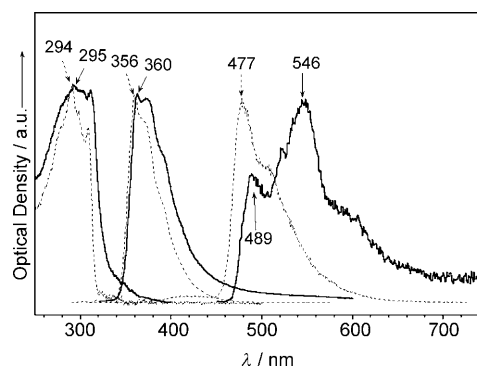


Figure 10. Absorption and emission (fluorescence and phosphorescence) spectra in the solid state (—) and in methycyclohexane solution (----) of **TEM**. The phosphorescence spectra both for solution and solid state were obtained at 77 K.

solid state. We see that the absorption and fluorescence spectra of **TEM** in thin films are slightly shifted to lower energies relative to the spectra in solution. Phosphorescent profiles are rather different in solution compared to the solid phase. The first vibronic peak is displaced by 0.06 eV (i.e., 477 nm in methylcyclohexane and 489 nm in the solid) in the phosphorescent spectrum of **TEM** and by 0.03 eV (by 4 nm in Figure 10) in the fluorescent spectrum. In addition, the component at 546 nm becomes stronger in the solid, in contrast to that at 477 nm in solution.

This indicates that the absorbing and singlet emitting states both in solution and in the solid state have very similar structures. Although larger distortions in solution relative to the solid would be expected, the small differences in the spectra indicate that the molecules keep almost the same molecular conformations (close-to-planarity conformers) in both phases, thus supporting the choice of planar C_{3h} models for the theoretical studies. In view of the alteration of the vibronic profile, this does not appear to be valid for the triplet state. Solid-state packing would tend to planarize the molecules, an effect that would likely have greater incidence than in solution phase on the triplet state owing to its significant cumulenization (i.e., cumulenization would be facilitated in a pro-planar solid-state environment).

As expected, the solid-state fluorescence quantum yields decrease by about one order of magnitude relative to the liquid phase; this decrease is more marked in **TEB** and more modest in **TEBF** (from 0.07 to 0.04), indicating that internal conversion for **TEBF** is already efficient in solution. In solid **TEB**, the effect of intermolecular interactions (i.e., solid-state aggregation) reduces the emission activity, hence leading to the largest changes of Φ_{fl} . In **TEM**, intermolecular packing is expected to be less favorable with respect to **TEB** because the three methyl groups in the molecular core introduce steric hindrance; this is consistent with the moderate change of Φ_{fl} . Moreover, the radiative and radiationless rate constant values did not change significantly relative to the solution behavior (Tables 3 and 5), which once more indicates that the deactivation pathways are identical in both liquid and solid media.

Table 5. Fluorescence and phosphorescence data as well as the rate constants in the solid state.

	$\lambda_{\text{max}}(\text{em fl})$ [nm]	$\lambda_{\text{max}}(\text{em ph})$ [nm]	Φ_{fl}	τ_{fl} [ns]	τ_{ph} [ms]
TEM	360, 375	489	0.03	5.74	115
TEB	355, 369	482	0.06	5.56	218
TEBF	365	480	0.04	2.54	248

Vibrational Raman spectra: Figure 11 shows the FT-Raman spectra of the three molecules in the solid state with an excitation wavelength of 1064 nm. It is possible to correlate the Raman frequencies with the molecular structure of the S_0 ground electronic state. As a representative case, Figure 12 displays the FT-Raman spectra of **TEB** between -170°C and 170°C in the solid state.

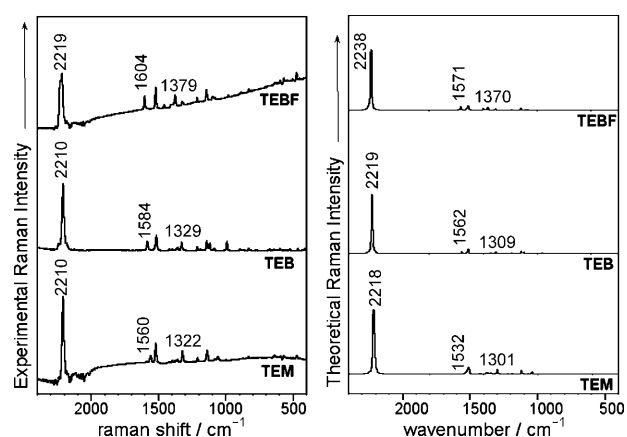


Figure 11. Left: 1064 nm FT-Raman spectra of the three compounds in the solid state. Right: DFT//B3LYP/6-31G** Raman spectra of the three compounds.

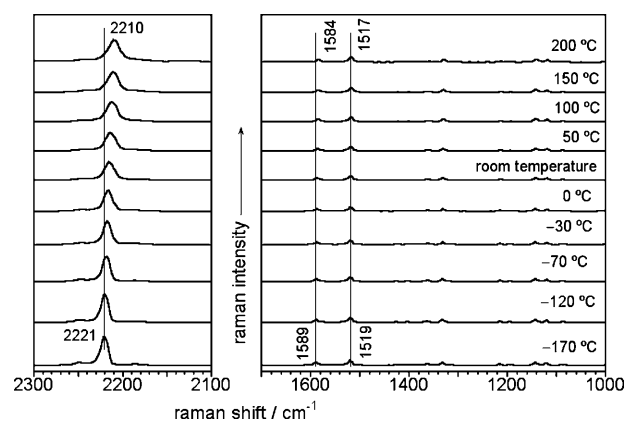


Figure 12. 1064 nm FT-Raman spectra of **TEB** as a function of the temperature.

The prominent bands in the three spectra are recorded at 2210 cm^{-1} in **TEB** and **TEM** and at 2219 cm^{-1} in **TEBF**. They are related to the $\text{C}\equiv\text{C}$ stretching vibration of the acetylene spacer. This assignment allows us to establish a structure–property relationship because the corresponding triple bond is significantly shorter in **TEBF**, in agreement with its larger vibrational frequency: 2210 cm^{-1} (**TEB**) \rightarrow 2210 cm^{-1} (**TEM**) \rightarrow 2219 cm^{-1} (**TEBF**) and 1.216 \AA (**TEB**) \rightarrow 1.217 \AA (**TEM**) \rightarrow 1.215 \AA (**TEBF**).

The stretching modes of the CC bonds of the central benzene ring appear in the $1600\text{--}1550\text{ cm}^{-1}$ spectral region. There is also a direct relationship between this vibrational frequency evolution and the CC bond lengths: 1584 cm^{-1} (**TEB**) \rightarrow 1560 cm^{-1} (**TEM**) \rightarrow 1604 cm^{-1} (**TEBF**) and $1.406/1.405\text{ \AA}$ (**TEB**) \rightarrow $1.410/1.417\text{ \AA}$ (**TEM**) \rightarrow 1.404 \AA (**TEBF**). As for the medium intensity lines at 1322 cm^{-1} in **TEM**, 1329 cm^{-1} in **TEB**, and 1379 cm^{-1} in **TEBF**, they can be described as C–C stretching modes of the single bonds of the spacers, or $\nu(\text{C–C})$. Their wavenumber values correlate well with the bond lengths calculated for the CC bonds connected to the core: 1.428 \AA (**TEM**), 1.426 \AA (**TEB**), and 1.418 \AA

(**TEBF**). The Raman data related to $\nu(\text{C}-\text{C})$ and $\nu(\text{C}\equiv\text{C})$ reflect the cumulenic character of the spacer in **TEBF** as a result of ground-state polarization by donor–acceptor interactions; this has a significant impact on the spectroscopic and NLO properties (vide infra).

These correlations highlight the possibility of tuning the spectroscopic properties as a function of the core substitution. As for the ground electronic state, **TEBF** can be viewed as a central acceptor core competing with three surrounding ethynyl groups that are also electron-withdrawing moieties. As a consequence, the S_0 electronic polarization is limited owing to partial cancellation of opposite effects. The contrary is expected in **TEM** because +I inductive electron donation of the methyl groups facilitates polarization of the benzene groups and of the acetylene spacers; overall **TEM** displays the largest/lowest bond lengths/Raman frequencies. It must be pointed out that although Raman data show a collapse of the electronic polarization in **TEBF**, the UV/Vis results indicate that this compound displays some charge-transfer character. Obviously, Raman frequencies reflect the S_0 molecular structure, whereas the electronic spectroscopic data are related to the $S_0 \rightarrow S_2/S_3$ or $S_1 \rightarrow S_0$ electronic excitations or relaxations.

The temperature evolution of the Raman frequencies in the solid state primarily indicates that the molecule has significant thermal stability; the spectra fully recover after heating to 200 °C (i.e., no appreciable changes are observed after thermal cycling). A continuous downshift is recorded with temperature for all the CC stretching bands that are involved in the π system; the most pronounced variation is observed for the $\nu(\text{C}\equiv\text{C})$ band at $\approx 2200 \text{ cm}^{-1}$, which shifts by -11 cm^{-1} . This behavior has been found for other π -conjugated molecules and planar molecules, and ascribed to the relatively small expansion/compression of the solid during the heating/cooling cycle resulting in the decrease/increase of the molecular interactions.^[36] A decrease of these interactions would soften the slope of the potential energy surface of the ground electronic state causing the vibrational frequencies to decrease. This interpretation agrees reasonably well with the possible formation of aggregates for these molecules.^[8]

Nonlinear optical spectroscopy: Owing to the octopolar nature of the investigated compounds, hyper Rayleigh scattering (HRS) is the method of choice for determining the first hyperpolarizability β .^[11] As expected from the linear one-photon fluorescence spectra, all three compounds exhibit significant (multiphoton) fluorescence when excited with strong IR pulses. Here, frequency-resolved femtosecond HRS with fluorescence demodulation at 800 nm has been applied.^[11] As a reference value, $330 \times 10^{-30} \text{ esu}$ was used for β_{xxx} of the octopolar molecule crystal violet in methanol, also at 800 nm. Upon simultaneously fitting the demodulation and the phase data as a function of modulation frequency, the fluorescence-free hyperpolarizability values were obtained together with the multiphoton fluorescence contribution, and the fluorescence lifetime (Table 1).

At the highest modulation frequencies, the fluorescence contribution is almost completely demodulated. Thus, an accurate value for the first hyperpolarizability can be obtained. The reported hyperpolarizability values are the dynamic, fluorescence-free values at 800 nm ($\beta_{\text{xxx},800}$) and the static, dispersion-free values ($\beta_{\text{xxx},0}$), as calculated using the three-level model.^[11] The depolarization ratios ρ obtained for the target compounds, referenced to the value for crystal violet, prove their octopolar symmetry, which in theory amounts to a value of 1.5. There exists a subtle modulation of β (either β_{000} or β_{xxx}) as a function of the substitution pattern. It shows the largest activity for **TEBF** in accordance with the charge-transfer interaction between the active excited states.

The components of the β tensor along the x axis (β_{xxx}), which is taken along one of the arms of the octopolar compounds, were calculated using two complementary approaches, the sum-over-states (SOS) method (see, e.g., ref. [26]) and the finite-field (FF) method.^[30a] The results are given in Table 6. The agreement among the values obtained

Table 6. Theoretical static β_{xxx} components of the first hyperpolarizability calculated with the SOS and FF methods for **TEBF**, **TEB**, and **TEM**.^[a]

Compound	$\beta_{\text{xxx}0} [10^{-30} \text{ esu}]$ exptl ^[b]	$\beta_{\text{xxx}} [10^{-30} \text{ esu}]$ FF	$\beta_{\text{xxx}} [10^{-30} \text{ esu}]$ SOS INDO/SCI ^[c]	$\beta_{\text{xxx}} 10^{-30} \text{ esu}]$ SOS INDO/SDCI ^[d]
TEBF	21 ± 1	15	18	11
TEB	7 ± 1	2	8	4
TEM	11 ± 1	3	1	1

[a] Absolute values. [b] HRS data obtained in CH_2Cl_2 , units in 10^{-30} esu . [c] All the π -molecular orbitals (MOs) were active in the SCI procedure. [d] Configuration interaction here includes single (S) excitations between all occupied and unoccupied π -MOs, and double (D) excitations among the five highest occupied π -MOs and five lowest unoccupied π^* -MOs.

with the two different approaches is good. Compared to experiments, the FF results reproduce the experimental trends better; the two methods provide the largest β values for **TEBF**, which is in agreement with experiment and with our assertion that the fluorine atoms exert an electron-withdrawing effect, in combination with the electron-richness of the terminal thienyl groups. This charge transfer can be viewed as a donor-to-acceptor electron polarization. The inductive effect of the three methyl groups, which causes the hyperpolarizability to increase very slightly from **TEB** to **TEM**, is well reproduced by the FF approach. The inclusion of the acceptor groups (-F) into the central benzene ring appears to be a crucial structural modification responsible for the large β_{xxx} component in **TEBF**.

In order to gain deeper insight into structure–property relationships, the calculated bond-length alternation (BLA) values and the HOMO–LUMO energy gap (ΔE) are discussed and displayed for **TEBF**, **TEB**, and **TEM** in Table 7. BLA was calculated by subtracting the triple bond length of the conjugation bridge from the average length of the two C–C bonds connected to it. The inclusion of the fluorine

Table 7. Experimental β_{xxx} values and theoretical DFT//B3LYP/6-31G** BLA values, HOMO and LUMO gaps (ΔE) for the thienyl-substituted benzene derivatives.

Compound	β_{xxx0} [10^{-30} esu] exper. ^[a]	BLA [\AA]	ΔE ^[b]
TEBF	21 ± 1	0.203	4.212
TEB	7 ± 1	0.207	4.253
TEM	11 ± 1	0.207	4.181

[a] HRS data obtained in CH_2Cl_2 , units in 10^{-30} esu. [b] $\Delta E = E_{\text{LUMO}} - E_{\text{HOMO}}$ in eV.

groups in the central benzene core decreases the lengths of the single CC bonds and increases the length of the triple CC bond, thus resulting in a decrease in the calculated BLA values. As expected from Table 7, a decrease in BLA and ΔE within the (-F) substitution of the benzene core leads to an increase in β .

Conclusion

We have synthesized three new molecules comprising three thieno-acetylene arms substituting a central benzene core with different electron donor/acceptor groups in the free phenyl positions. The absorption and fluorescence properties are consistent with the fact that the absorbing and emitting states are different, as a consequence of the C_3 planar (i.e., C_{3h}) molecular symmetry. Fine modulation of these properties is observed as a result of chemical functionalization of the central core; however, such a modulation does not occur for the ground electronic properties, as observed from Raman spectroscopy data, which show the intrinsic effect of donor–acceptor (**TEB** and **TEM**) and acceptor–acceptor (**TEBF**) interactions.

The photophysical properties are satisfactorily explained by the coupling of the singlet and triplet manifolds. We find ISC to be an important de-excitation route, based on the measurements of the phosphorescence spectra and triplet-state formation quantum yields. The molecules can be considered as rather good phosphorescent dyes given the low propensity of pure π , π^* states to phosphoresce. As a result, the internal conversion route coupled to the ground electronic state seems to be a competitive mechanism with fluorescence and phosphorescence. In all the cases, we have provided theoretical support for our conclusions. As for the hyperpolarizabilities, these are moderate and display a typical dependence on the donor–acceptor substitution pattern.

In summary, a complete study of the nature of the electronic states in new molecules has been carried out. It describes interesting molecular properties directed to the understanding of the structure of their low-lying excited states. These molecular features are responsible for their performance in organic electronics, such as in nonlinear optical and light-emitting devices. Comprehensive analyses, such as those carried out here, are needed in order to design advanced or improved molecules from a property–function point of view.

Acknowledgements

The present work was supported in part by the Dirección General de Enseñanza Superior (DGES, MEC, Spain) through research projects CTQ2006-14987-C02-01 and CT2007-65683. The authors are also indebted to Junta de Andalucía for the project FQM1678/2006. J.C. and G.H. are grateful to the MEC of Spain for I3 professorships. M.M.O. is indebted to the MEC for a predoctoral FPU fellowship. J.S.D.M. acknowledges financial support from the Portuguese Science Foundation (FCT) through FEDER and POCI. MCRD acknowledges the MEC for a MEC/Fulbright Postdoctoral Fellowship at the Georgia Institute of Technology. The work at Georgia Tech was partly supported by the STC Program of the National Science Foundation (Award DMR-0120967).

- [1] a) A. Tsumura, H. Koezuka, T. Ando, *Appl. Phys. Lett.* **1986**, *49*, 1210; b) C. D. Dimitrakopoulos, P. Malenfant, *Adv. Mater.* **2002**, *14*, 99; c) J. A. Rogers, Z. Bao, A. Dodabalapur, B. Crone, V. R. Raju, H. E. Katz, V. Kuck, K. J. Ammundson, P. Drzaic, *Proc. Natl. Acad. Sci. USA* **2001**, *98*, 4817; d) F. Garnier, *Acc. Chem. Res.* **1999**, *32*, 209; e) J. H. Burroughes, D. D. C. Bradley, R. N. Marks, R. H. Friend, P. L. Burn, A. B. Holmes, *Nature* **1990**, *347*, 539; f) A. Kraft, A. C. Grimsdale, A. B. Holmes, *Angew. Chem.* **1998**, *110*, 416; *Angew. Chem. Int. Ed.* **1998**, *37*, 402; g) U. Mitschke, P. Bäuerle, *J. Mater. Chem.* **2000**, *10*, 1471; h) H. Sirringhaus, *Adv. Mater.* **2005**, *17*, 2411; i) J. Roncali, P. Leriche, A. Cravino, *Adv. Mater.* **2007**, *19*, 2045; j) T. Noda, H. Ogawa, N. Noma, Y. Shirota, *J. Mater. Chem.* **1999**, *9*, 2177; k) A. Facchetti, M. Musher, H. E. Katz, T. J. Marks, *Adv. Mater.* **2003**, *15*, 33; l) V. Coropceanu, J. Cornil, D. A. Da Silva Filho, Y. Olivier, R. Silbey, J.-L. Bredas, *Chem. Rev.* **2007**, *107*, 926.
- [2] a) C. Bosshard, K. Sutter, P. Prêtre, J. Hulliger, M. Flörshimer, P. Kaatz, P. Günther, *Organic Nonlinear Optical Materials, Vol. 1*, Gordon & Breach, Amsterdam, **1995**; b) F. Meyers, S. R. Marder, J. W. Perry in *Chemistry of Advanced Materials: An Overview* (Eds.: L. V. Interrante, M. J. Hamden-Smith), Wiley-VCH, Weinheim, **1998**; c) T. Verbiest, K. Clays, C. Samyn, J. Wolff, D. Reinhoudt, A. Persoons, *J. Am. Chem. Soc.* **1994**, *116*, 9320; d) J. Zyss, *J. Chem. Phys.* **1993**, *98*, 6583; e) J. Zyss, I. Ledoux, *Chem. Rev.* **1994**, *94*, 77.
- [3] a) L. Porrès, O. Mongin, C. Katan, M. Charlot, T. Pons, J. Mertz, M. Blanchard-Desce, *Org. Lett.* **2004**, *6*, 47–50; b) W.-H. Lee, H. Lee, J.-A. Kim, J.-H. Choi, M. Cho, S.-J. Jeon, B. R. Cho, *J. Am. Chem. Soc.* **2001**, *123*, 10658; c) G. S. He, J. Swiatkiewicz, Y. Jiang, P. N. Prasad, B. A. Reinhardt, L. S. Tan, R. Kannan, *J. Phys. Chem. A* **2000**, *104*, 4805–4810; d) C. Katan, F. Terenziani, O. Mongin, M. H. V. Werts, L. Porres, T. Pons, J. Mertz, S. Tretiak, M. Blanchard-Desce, *J. Phys. Chem. A* **2005**, *109*, 3024–3037; e) G. Bordeau, R. Lartia, G. Metge, C. Fiorini-Debuisschert, F. Charra, M. P. Teulade-Fichou, *J. Am. Chem. Soc.* **2008**, *130*, 16836–16837; f) D. Beljonne, W. Wenseleers, E. Zojer, Z. Shuai, H. Vogel, S. J. K. Pond, J. W. Perry, S. R. Marder, J. L. Brédas, *Adv. Funct. Mater.* **2002**, *12*, 631.
- [4] a) A. Cravino, S. Roquet, O. Aleveque, P. Leriche, P. Frere, J. Roncali, *Chem. Mater.* **2006**, *18*, 2584; b) R. de Bettignies, Y. Nicolas, P. Blanchard, E. Levillain, J.-M. Nunzi, J. Roncali, *Adv. Mater.* **2003**, *15*, 1939; c) F. Chérioux, L. Guyard, P. Audebert, *Chem. Commun.* **1998**, 2225; d) J. Bras, S. Guillerez, Pépin-B. Donat, *Chem. Mater.* **2000**, *12*, 2372; e) Y. Geng, A. Fechtenkötter, K. Müllen, *J. Mater. Chem.* **2001**, *11*, 1634; f) T. M. Pappenfus, K. R. Mann, *Org. Lett.* **2002**, *4*, 3043–3046; g) S. A. Ponomarenko, S. Kirchmeyer, A. Elschner, B.-H. Huisman, A. Karbach, D. Drechsler, *Adv. Funct. Mater.* **2003**, *13*, 591; h) S. A. Ponomarenko, E. A. Tatarinova, A. M. Muzafarov, S. Kirchmeyer, L. Brassat, A. Mourran, M. Moeller, S. Setayesh, D. De Leeuw, *Chem. Mater.* **2006**, *18*, 4101; i) M. Y. Cho, S. J. Kim, D. Y. Han, D. H. Park, K. H. Kim, D. H. Choi, J. Joo, *Adv. Funct. Mater.* **2008**, *18*, 2905; j) K. Kreger, M. Baete, C. Neuber, H.-W. Schmidt, P. Strohriegel, *Adv. Funct. Mater.* **2007**, *17*, 3456.
- [5] a) M. Moreno Oliva, J. Casado, J. T. Lopez Navarrete, G. Henrich, M. C. Ruiz Delgado, J. Orduna, *J. Phys. Chem. C* **2007**, *111*, 18778; b) M. C. Ruiz Delgado, J. Orduna, M. Moreno Oliva, J. Casado, J. T.

- Lopez Navarrete, *J. Chem. Phys.* **2007**, *127*, 164704; c) M. Moreno Oliva, J. Casado, J. T. Lopez Navarrete, R. Berridge, P. J. Skabar, A. L. Kanibolotsky, Perepichka, F. Igor, *J. Phys. Chem. B* **2007**, *111*, 4026; d) M. Moreno Oliva, J. Casado, G. Hennrich, J. T. Lopez Navarrete, *J. Phys. Chem. B* **2006**, *110*, 19198.
- [6] Y. Tu, Y. Luo, H. Ågren, *J. Phys. Chem. B* **2005**, *109*, 16730.
- [7] V. Le Floch, S. Brasselet, J. Zyss, B. R. Cho, S. H. Lee, S.-J. Jeon, M. Cho, K. S. Min, M. P. Suh, *Adv. Mater.* **2005**, *17*, 196.
- [8] G. Hennrich, A. Omenat, I. Asselberghs, S. Foerier, K. Clays, T. Verbiest, J. L. Serrano, *Angew. Chem.* **2006**, *118*, 4310; *Angew. Chem. Int. Ed.* **2006**, *45*, 4203.
- [9] a) S. R. Marder, *Chem. Commun.* **2006**, 131; b) *Nonlinear Optical Properties of Matter: From Molecules to Condensed Phases* (Eds.: M. G. Papadopoulos, J. Leszczynski, A. J. Sadlej), Kluwer, Dordrecht, **2006**.
- [10] J. M. Seminario, A. G. Zarcarias, J. M. Tour, *J. Am. Chem. Soc.* **1998**, *120*, 3970.
- [11] a) K. Clays, K. Wostyn, A. Persoons, *Adv. Funct. Mater.* **2002**, *12*, 557; b) E. Hendrickx, K. Clays, A. Persoons, *Acc. Chem. Res.* **1998**, *31*, 675; c) G. Olbrechts, R. Strobbe, K. Clays, A. Persoons, *Rev. Sci. Instrum.* **1998**, *69*, 2233; d) K. Wostyn, K. Binnemans, K. Clays, A. Persoons, *Rev. Sci. Instrum.* **2001**, *72*, 3215.
- [12] R. Chinchilla, C. Nájera, *Chem. Rev.* **2007**, *107*, 874.
- [13] R. S. Becker, J. Seixas de Melo, A. L. Macanita, F. Elisei, *J. Phys. Chem.* **1996**, *100*, 18683.
- [14] J. Pina, H. D. Burrows, R. S. Becker, F. B. Dias, A. L. Macanita, J. Seixas de Melo, *J. Phys. Chem. B* **2006**, *110*, 6499.
- [15] G. Striker, V. Subramaniam, C. A. M. Seidel, A. Volkmer, *J. Phys. Chem. B* **1999**, *103*, 8612.
- [16] J. Pina, J. Seixas de Melo, H. D. Burrows, A. Bilge, T. Farrell, M. Forster, U. Scherf, *J. Phys. Chem. B* **2006**, *110*, 15100.
- [17] P. J. Stephens, F. J. Devlin, F. C. F. Chabalowski, M. J. Frisch, *J. Phys. Chem.* **1994**, *98*, 11623; J. J. Novoa, C. Sosa, *J. Phys. Chem.* **1995**, *99*, 15837; E. Casida, C. Jamorski, K. C. Casida, D. R. Salahub, *J. Chem. Phys.* **1998**, *108*, 4439; R. E. Stratmann, G. E. Scuseria, M. J. Frisch, *J. Chem. Phys.* **1998**, *109*, 8218.
- [18] E. Runge, E. K. U. Gross, *Phys. Rev. Lett.* **1984**, *52*, 997; E. K. U. Gross, W. Kohn, *Adv. Quantum Chem.* **1990**, *21*, 255; H. Heinze, A. Goerling, N. Roesch, *J. Chem. Phys.* **2000**, *113*, 2088.
- [19] J. B. Foresman, M. Head-Gordon, J. A. Pople, M. J. Frish, *J. Phys. Chem.* **1992**, *96*, 135.
- [20] Gaussian03, Revision B.05, M. J. Frisch, G. W. Trucks, H. B. Schlegel, G. E. Scuseria, M. A. Robb, J. R. Cheeseman, J. A. Montgomery, Jr., T. Vreven, K. N. Kudin, J. C. Burant, J. M. Millam, S. S. Iyengar, J. Tomasi, V. Barone, B. Mennucci, M. Cossi, G. Scalmani, N. Rega, G. A. Petersson, H. Nakatsuji, M. Hada, M. Ehara, K. Toyota, R. Fukuda, J. Hasegawa, M. Ishida, T. Nakajima, Y. Honda, O. Kitao, H. Nakai, M. Klene, X. Li, J. E. Knox, H. P. Hratchian, J. B. Cross, V. Bakken, C. Adamo, J. Jaramillo, R. Gomperts, R. E. Stratmann, O. Yazyev, A. J. Austin, R. Cammi, C. Pomelli, J. W. Ochterski, P. Y. Ayala, K. Morokuma, G. A. Voth, P. Salvador, J. J. Dannenberg, V. G. Zakrzewski, S. Dapprich, A. D. Daniels, M. C. Strain, O. Farkas, D. K. Malick, A. D. Rabuck, K. Raghavachari, J. B. Foresman, J. V. Ortiz, Q. Cui, A. G. Baboul, S. Clifford, J. Cioslowski, B. B. Stefanov, G. Liu, A. Liashenko, P. Piskorz, I. Komaromi, R. L. Martin, D. J. Fox, T. Keith, M. A. Al-Laham, C. Y. Peng, A. Nanayakkara, M. Challacombe, P. M. W. Gill, B. Johnson, W. Chen, M. W. Wong, C. Gonzalez, J. A. Pople, Gaussian, Inc., Pittsburgh, PA, **2003**.
- [21] A. D. Becke, *J. Chem. Phys.* **1993**, *98*, 1372.
- [22] M. M. Francl, W. J. Pietro, W. J. Hehre, J. S. Binkley, M. S. Gordon, D. J. Defrees, J. A. Pople, *J. Chem. Phys.* **1982**, *77*, 3654.
- [23] A. Pople, D. L. Beveridge, P. A. Dobosh, *J. Chem. Phys.* **1967**, *47*, 2026.
- [24] N. Mataga, K. Nishimoto, *Z. Phys. Chem.* **1957**, *13*, 140.
- [25] M. C. Zerner, G. H. Loew, R. F. Kichner, U. Mueller-Westerhoff, *J. Am. Chem. Soc.* **1980**, *102*, 589.
- [26] F. Meyers, S. R. Marder, B. M. Pierce, J. L. Brédas, *J. Am. Chem. Soc.* **1994**, *116*, 10703.
- [27] H. D. Cohen, C. C. J. Roothaan, *J. Chem. Phys.* **1965**, *43*, 34.
- [28] P. Chopra, L. Carlucci, H. F. King, P. N. Prasad, *J. Phys. Chem.* **1989**, *93*, 7120.
- [29] M. N. Nakano, I. Shigemoto, S. Yamada, K. Yamaguchi, *J. Chem. Phys.* **1995**, *103*, 4175.
- [30] a) V. M. Geskin, J. L. Brédas, *J. Chem. Phys.* **1998**, *109*, 6163; b) V. M. Geskin, C. Lambert, J. L. Brédas, *J. Am. Chem. Soc.* **2003**, *125*, 15651.
- [31] a) D. Beljonne, J. Cornil, R. H. Friend, R. A. J. Janssen, J. L. Brédas, *J. Am. Chem. Soc.* **1996**, *118*, 6453; b) D. Beljonne, Z. Shuai, R. H. Friend, J. L. Brédas, *J. Chem. Phys.* **1995**, *102*, 2042.
- [32] D. Wasserberg, P. Marsal, S. C. J. Meskers, R. A. J. Janssen, D. Beljonne, *J. Phys. Chem. B* **2005**, *109*, 4410.
- [33] R. S. Becker, *Theory and Interpretation of Fluorescence and Phosphorescence*, Wiley-Interscience, New York, **1969**.
- [34] N. J. Turro, *Modern Molecular Photochemistry*, University Science Books, Sausalito, **1991**.
- [35] R. A. J. Janssen, *Primary Photoexcitations in Conjugated Polymers* (Ed.: N. S. Sariciftci), World Scientific, Singapore, **1997**, pp. 524–558.
- [36] J. Casado, T. M. Pappenfus, K. R. Mann, E. Ortí, P. M. Viruela, B. Milián, V. Hernández, López J. T. Navarrete, *ChemPhysChem* **2004**, *5*, 529.

Received: March 18, 2009
Published online: July 16, 2009